Meteorol Atmos Phys (2018) 130:333–348
https://doi.org/10.1007/s00703-017-0533-x

ORIGINAL PAPER

Looping tracks associated with tropical cyclones approaching an isolated mountain. Part I: Essential parameters

Yi-Chih Huang[1] · **Yuh-Lang Lin**[2,3]

Received: 3 November 2016 / Accepted: 9 May 2017 / Published online: 15 May 2017

Abstract Essential parameters for making a looping track when a westward-moving tropical cyclone (TC) approaches a mesoscale mountain are investigated by examining several key nondimensional control parameters with a series of systematic, idealized numerical experiments, such as U/Nh, V_{max}/Nh, U/fL_x, V_{max}/fR, h/L_x, and R/L_y. Here U is the uniform zonal wind velocity, N the Brunt–Vaisala frequency, h the mountain height, f the Coriolis parameter, V_{max} the maximum tangential velocity at a radius of R from the cyclone center and L_x is the halfwidth of the mountain in the east–west direction. It is found that looping tracks (a) tend to occur under small U/Nh and U/fL_x, *moderate* h/L_x, and large V_{max}/Nh, which correspond to slow movement (leading to subgeostrophic flow associated with strong orographic blocking), moderate steepness, and strong tangential wind associated with TC vortex; (b) are often accompanied by an area of perturbation high pressure to the northeast of the mountain, which lasts for only a short period; and (c) do not require the existence of a northerly jet. The nondimensional control parameters are consolidated into a TC looping index (LI), $\frac{U^2R^2}{V_{max}^2hL_y}$, which is tested by several historical looping and non-looping typhoons approaching Taiwan's Central Mountain Range (CMR) from east or southeast. It is found that LI < 0.0125 may serve as a criterion for looping track to occur.

1 Introduction

When a tropical cyclone (TC) makes a looping track, its impacts on rainfall and gusty wind are dramatic and much stronger than a nonlooping TC. A TC may make a looping track when it is blocked by a synoptic cold front [e.g., Hurricanes Dennis (1999), Catarina (2004), Nadine (2012), etc.] or by a mesoscale mountain [e.g., Typhoons Fung-wong (2002), Haitang (2005), Krosa (2007), Sinlaku (2008), etc.]. In previous studies, several mechanisms have been proposed to explain looping tracks of typhoons when they approached Taiwan's Central Mountain Range (CMR), which include the *lee vortex-tropical cyclone interaction* (Yeh et al. 2012), the *channel effect* (Jian and Wu 2008; Huang et al. 2011), the *vortex–vortex interaction with another typhoon* (Zhang et al. 2011; Yang et al. 2008a), the *horizontal advection of potential vorticity* (Yu et al. 2007), and the advection by orographically blocked basic flow (Lin et al. 2016).

Jian and Wu (2008) investigated the looping track of Typhoon Haitang (2005) with the Weather Research and Forecasting (WRF) modeling simulations, which found that a low-level northerly jet is induced by the channeling effect between CMR and the TC vortex. The *channel effect* was induced by terrain, as originally proposed by Lin et al. (1999) for explaining the southward deflection of drifting vortex passing over CMR, which shifts the strongest winds of the storm to the western side of the eyewall. Based on real-case and idealized simulations of Typhoon Krosa

Responsible Editor: M. Kaplan.

✉ Yi-Chih Huang
dscpln@gate.sinica.edu.tw

[1] Research Center for Environmental Changes, Academia Sinica, 128 Academia Road, Section 2, Nankang, Taipei 115, Taiwan

[2] Department of Physics, North Carolina A&T State University, Greensboro, NC, USA

[3] Department of Energy and Environmental Systems, North Carolina A&T State University, Greensboro, NC, USA

(2007), Huang et al. (2011) found that strong channel winds were intensified between the storm and the topography just before looping occurred. The mountain height was considered as the most important factor in causing the looping track, compared to surface properties, details of topographic shapes, and cloud microphysics. Using piecewise potential vorticity inversion analysis and numerical model simulations, Yeh et al. (2012) attributed the Haitang's looping to the binary vortex interaction in which a CMR-induced lee vortex and Typhoon Haitang (2005) rotate around their system centers. This lee vortex–TC interaction mechanism suffers from the fact that when a westward TC approaches Taiwan's CMR, lee vortex and northerly jet are often observed, but not looping tracks. Note that it takes time for a lee vortex to develop when a TC approaches CMR, which may propose a causality problem even though intuitively the *lee vortex–TC interaction mechanism* seems working, however, there might be a causality problem.

Employing the potential vorticity diagnosis of numerically simulated results, Yang et al. (2008a) researched the *binary interaction* of Typhoons Fengshen (2002) and Fungwong (2002). They found that in the earlier stage, the looping of Typhoon Fungwong (2002) is mainly forced by Typhoon Fengshen (2002). Then a mutual interaction occurs in the later stages. Additionally, the monsoon trough and subtropical high pressure play a role in the binary interaction. Utilizing large-scale analyses, satellite observations, and a nested, cloud-resolving simulation, Zhang et al. (2011) showed that the vortex–vortex interaction with Typhoon Danas (2001) resulted in the looping track of Typhoon Nari (2001). The interaction between Kuroshio Current and the *vortex–vortex interaction* controls the variable intensity of Typhoon Nari (2001) during the looping. The vortex–vortex interaction also obstructs Nari accessing convective available potential energy in the large-scale environment. While the vortex–vortex interaction mechanism may work, it is not a necessary condition since TC looping did occur without the existence of two nearby typhoons, such as Haitang (2005), Krosa (2007), Sinlaku (2009), etc.

Based on a typhoon model and potential vorticity (PV) budget analysis of numerical simulations of Typhoon Haitang (2005), Yu et al. (2007) shed some lights on the understanding of the movement of its looping track. Most of the time, the center of Haitang moves to the region of maximum wavenumber one PV tendency, which is predominantly caused by the *horizontal advection and diabatic heating*. The mid-level warm air intrusion and the breakouts of low-level southwesterly jet lead to phase-lock diabatic heating on the PV tendency field that eventually gives rise to the looping track of Haitang. The sensitivity experiment suggested that the CMR may not be a crucial factor. The *horizontal advection and diabatic heating mechanism* proposed by Yu et al. (2007) for the looping track is appealing, nonetheless, a couple of questions may be raised: why are the two loopings over Taiwan Strait simulated by Yu et al. so different from observations, and so much more distinct from the looping before landfall on Taiwan? Is it possible that the unusual looping track was generated by the specific setting in the numerical simulations? The sensitivity numerical experiments in Yang et al. (2008b) showed that looping tracks were explained by the environmental steering flows when the height of CMR was systematically increased. However, the dramatic change of the steering flow from the control run to that with 75% terrain height remains unexplained. Therefore, mechanisms for TC looping should be regarded as still not well understood.

In summary, the key question for TC looping is: what are the environments conducive to the formation of TC looping, or, specifically, what are the essential dimensional and/or nondimensional parameters of the TC looping tracks when a TC approaches a mesoscale mountain? Nondimensional parameters can simplify the governing equations, provide insight on controlling factors and the nature of the problem, and help predict the occurrence of TC looping. The investigation of nondimensional parameters can be applied to various TC cases rather than only for a specific case. Previously some key nondimensional parameters have been proposed to explain TC track deflection and discontinuity (e.g., Lin et al. 1999, 2005). In this study, we plan to conduct numerical simulations to investigate the ranges of essential nondimensional and dimensional parameters associated with the TC looping. This will enhance our understanding of the mechanisms for TC looping tracks caused by orographic forcing. Furthermore, based on the essential nondimensional parameters and dimensional variables, we will consolidate these parameters to construct a looping index for TCs.

The rest of this paper is organized as follows. The model description and numerical experimental design can be found in Sect. 2. In Sect. 3, we will discuss the ranges of nondimensional parameters which control the TC looping, the related regimes, basic physical fields, and a looping index. Conclusions are in the Sect. 4.

2 Numerical model description, and numerical experiment design

2.1 Model description

The numerical model utilized in this research is the Geophysical Fluid Dynamics Model (GFDM) as described in Lin et al. (1999), which is based on three-dimensional,

primitive equations for a dry, stratified, hydrostatic, and Boussinesq fluid. There is no cloud physics and planetary boundary layer included in this model. The governing equations of the models are in the terrain-following coordinates (Gal-Chen and Sommerville 1975) and the characteristics of the GFDM are briefly summarized as follows:

- The atmospheric variables are arranged on an Arakawa C staggered grid.
- The third-order Adams–Bashforth scheme is used in time integration.
- The horizontal and vertical advection schemes are fourth-order and second-order centered difference schemes, respectively.
- The vertical coordinate is a terrain-following one defined as $\sigma = z_T(z - h)/(z_T - h)$, where z_T is the height of vertical domain, and h is the terrain elevation.
- The lower boundary condition is free-slip.
- The upper boundary condition is a radiation boundary condition (Klemp and Durran 1983).
- Orlanski (1976) radiation condition is used as the lateral boundary condition.
- Subtracting off the horizontal average of pressure reduces truncation error due to topographic terms and diminishes the unrealistic pressure perturbation (Clark 1977).
- A five-point numerical smoothing is employed in both horizontal and vertical directions (Shapiro 1970).

The initial potential temperature field in GFDM depends on the basic flow field. For example, when the basic flow contains constant Brunt–Vaisala frequency (N) and uniform zonal wind velocity (U), the potential temperature θ can be calculated from the definition of N, i.e. $N^2 = \frac{g}{\theta}\frac{\partial\bar{\theta}}{\partial z}$ where $\bar{\theta}$ is given as 273 K at the lowest level. When the Brunt–Vaisala frequency is constant with height and the basic wind shear is linear with height, the potential temperature is given by the thermal wind balance $U_z = -\frac{g}{f\theta}\frac{\partial\bar{\theta}}{\partial y}$. The numerical formulation of the model can be found in Lin et al. (1999).

2.2 Numerical experiment design

A uniform stably stratified basic flow is assumed for all simulations conducted in this study. The numerical experiments are designed for a uniform easterly flow with constant Brunt–Vaisala frequency ($N = 0.01\ \mathrm{s}^{-1}$) over a bell-shaped topography as represented in Eq. (1) of mountain height (h), zonal half-width (a), and meridional half-width (b) on an f-plane approximation ($f = 5.8 \times 10^{-5}\ \mathrm{s}^{-1}$). Note that $2a$ and $2b$ are used to represent zonal and meridional horizontal scales of mountain L_x and L_y, respectively.

$$H(x,y) = \frac{h}{\left(\frac{x^2}{a^2} + \frac{y^2}{b^2} + 1\right)^{3/2}}. \quad (1)$$

An idealized bogus vortex is initialized with a prescribed tangential velocity as Eq. (2) from Chang (1982).

$$V(r) = V_{\max}\left(\frac{r}{R}\right)\exp\left\{\frac{1}{2}\left[1 - \left(\frac{r}{R}\right)^2\right]\right\}, \quad (2)$$

where $V_{\max}$ is the maximum tangential velocity at a radius of R from the cyclone center. A nonlinear, nondivergent initialization is applied to obtain the velocity, pressure, and potential temperature fields of the cyclone. The final balanced velocity field is nondivergent and in gradient wind balance. The initialization processes, vertical profile of $V_{\max}$, and horizontal structure of surface pressure perturbation, surface vertical vorticity, and wind vectors can be found in Lin et al. (1999). Because latent heating is not included in the model, the cyclone vortices in simulations are given relatively larger radii of maximum tangential wind to avoid having barotropic instability.

The horizontal grid interval is set to $\Delta x = \Delta y = 10$ km, while the vertical grid interval is 500 m. The numbers of grid points are 301 × 241 × 31 in the three-dimensional domain 3000 km × 2400 km × 15 km. In the beginning the vortex is set at $(x/a,\ y/a) = (7.5,\ 0)$ in all cases. The track is traced by the maximum vorticity center.

In this study, we conducted a series of numerical experiments to identify which nondimensional (or dimensional) parameter is important for the looping track in a westward moving cyclone. The key parameters of TC approaching a mesoscale mountain in the concerned question are the basic flow speed (U), maximum tangential wind speed of the TC ($V_{\max}$), meridional mountain scale (L_y), zonal mountain scale (L_x), mountain height (h), radius of $V_{\max}$ (R), Brunt–Vaisala frequency (N), and Coriolis parameter (f). We hypothesize that a looping track is closely related to the orographic blocking of a TC. The nondimensional parameters, i.e. U/Nh, $V_{\max}/Nh$, U/fL_x, $V_{\max}/fR$, h/L_x, and R/L_y, were used to study the relation between looping tracks and orographic blocking. Note that the nondimensional parameters U/Nh, $V_{\max}/Nh$, U/fL_x, $V_{\max}/fR$, h/L_x, and R/L_y have been defined as the basic-flow Froude number, vortex Froude number, Eulerian Rossby number, Lagrangian Rossby number of a TC, the steepness of a mountain, and the aspect ratio of the cyclone scale to the terrain scale perpendicular to the cyclone movement, respectively.

We started with the control experiment which has $U = 5\ \mathrm{m\ s}^{-1}$, $V_{\max} = 30\ \mathrm{m\ s}^{-1}$, $L_y = 480$ km, $L_x = 80$ km, $h = 3.75$ km, and $R = 90$ km, and adjusted values of the parameters systematically to search for the conditions under which looping occurs. All the dimensional and nondimensional parameters, along with the associated

Table 1 Dimensional and nondimensional parameters in the numerical experiments

Case	U (ms^{-1})	V_{max} (ms^{-1})	L_y (km)	L_x (km)	h (km)	R (km)	U/Nh	V_{max}/Nh	U/fL_x	V_{max}/fR	h/L_x	R/L_y	L/N
CTL	5	30	480	80	3.75	90	0.13	0.8	1.08	5.75	0.047	0.188	N
A4	2.5	30	480	80	3.75	90	0.067	0.8	0.539	5.75	0.047	0.188	N
A5	1.5	30	480	80	3.75	90	0.040	0.8	0.323	5.75	0.047	0.188	N
A6	1	30	480	80	3.75	90	0.027	0.8	0.216	5.75	0.047	0.188	N
A7	0.5	30	480	80	3.75	90	0.013	0.8	0.108	5.75	0.047	0.188	L
C1	2.5	30	480	80	3.0	90	0.083	1.0	0.539	5.75	0.038	0.188	N
C2	2.5	30	480	80	2.5	90	0.10	1.2	0.539	5.75	0.031	0.188	N
C3	2.5	30	480	80	2.0	90	0.125	1.5	0.539	5.75	0.025	0.188	N
C4	2.5	30	480	80	1.0	90	0.25	3.0	0.539	5.75	0.013	0.188	N
C5	1.5	30	480	80	2.0	90	0.075	1.5	0.323	5.75	0.025	0.188	N
C6	1.5	30	480	80	1.5	90	0.10	2.0	0.323	5.75	0.019	0.188	N
C7	1	30	480	80	3.0	90	0.033	1.0	0.216	5.75	0.038	0.188	N
C8	1	30	480	80	2.5	90	0.04	1.2	0.216	5.75	0.031	0.188	N
C9	1	30	480	80	2.0	90	0.05	1.5	0.216	5.75	0.025	0.188	N
C10	1	30	480	80	1.5	90	0.067	2.0	0.216	5.75	0.019	0.188	L
C11	1	30	480	80	1.2	90	0.083	2.5	0.216	5.75	0.015	0.188	N
C12	1	30	480	80	1.0	90	0.1	3.0	0.216	5.75	0.013	0.188	N
C13	0.5	30	480	80	3.0	90	0.017	1.0	0.108	5.75	0.038	0.188	L
C14	0.5	30	480	80	2.5	90	0.02	1.2	0.108	5.75	0.031	0.188	L
C15	0.5	30	480	80	2.0	90	0.025	1.5	0.108	5.75	0.025	0.188	L
C16	0.5	30	480	80	1.5	90	0.033	2.0	0.108	5.75	0.019	0.188	L
C17	0.5	30	480	80	1.2	90	0.042	2.5	0.108	5.75	0.015	0.188	L
C18	0.5	30	480	80	1.0	90	0.050	3.0	0.108	5.75	0.013	0.188	N
C19	0.25	30	480	80	1.2	90	0.021	2.5	0.0539	5.75	0.015	0.188	L
C20	0.25	30	480	80	1.0	90	0.025	3.0	0.0539	5.75	0.013	0.188	N
D6	1	10	480	80	3.0	90	0.033	0.33	0.216	1.92	0.038	0.188	N
D7	1	10	480	80	2.5	90	0.04	0.4	0.216	1.92	0.031	0.188	N
D8	1	50	480	80	3.75	90	0.027	1.33	0.216	9.58	0.047	0.188	N
D9	1	50	480	80	3.0	90	0.033	1.67	0.216	9.58	0.038	0.188	N
D10	1	50	480	80	2.5	90	0.04	2.0	0.216	9.58	0.031	0.188	L
D11	1	40	480	80	2.5	90	0.04	1.6	0.216	7.66	0.031	0.188	N
D12	1	20	480	80	2.5	90	0.04	0.8	0.216	3.83	0.031	0.188	N
D13	0.5	10	480	80	2.5	90	0.02	0.4	0.108	1.92	0.031	0.188	N
E4	1	30	960	80	3.75	90	0.027	0.8	0.216	5.75	0.047	0.0938	N
E5	1	30	960	80	3.0	90	0.033	1.0	0.216	5.75	0.038	0.0938	N
E6	1	30	960	80	2.5	90	0.040	1.2	0.216	5.75	0.031	0.0938	L
E7	1	30	960	80	2.5	60	0.040	1.2	0.216	8.62	0.031	0.0625	N
E8	1	30	720	80	2.5	90	0.040	1.2	0.216	5.75	0.031	0.125	N
E9	1	30	480	80	2.5	90	0.040	1.2	0.216	5.75	0.031	0.188	N
E10	1	30	360	80	2.5	90	0.040	1.2	0.216	5.75	0.031	0.250	N
E11	1	30	300	80	2.5	90	0.040	1.2	0.216	5.75	0.031	0.300	L
E12	1	30	240	80	2.5	90	0.040	1.2	0.216	5.75	0.031	0.375	N
E13	1	30	180	80	2.5	90	0.040	1.2	0.216	5.75	0.031	0.500	N
F4	1	30	480	40	3.75	90	0.026	0.8	0.431	5.75	0.094	0.188	N
F5	1	30	480	40	3	90	0.033	1	0.431	5.75	0.075	0.188	L
F6	1	30	480	160	2.5	90	0.040	1.2	0.108	5.75	0.016	0.188	N
F7	1	30	480	120	2.5	90	0.040	1.2	0.144	5.75	0.021	0.188	N
F8	1	30	480	40	2.5	90	0.040	1.2	0.431	5.75	0.063	0.188	L

Table 1 continued

Case	U (ms^{-1})	V_{max} (ms^{-1})	L_y (km)	L_x (km)	h (km)	R (km)	U/Nh	V_{max}/Nh	U/fL_x	V_{max}/fR	h/L_x	R/L_y	L/N
F9	0.5	30	480	40	3	90	0.017	1	0.216	5.75	0.075	0.188	L
F10	0.5	30	480	40	2.5	90	0.020	1.2	0.216	5.75	0.063	0.188	L

U, V_{max}, L_y, L_x, h, and R are basic flow speed, maximum tangential wind speed of the tropical cyclone, meridional mountain scale, zonal mountain scale, mountain height, and the radius of V_{max}, respectively. The Brunt–Vaisala frequency (N) is 0.01 s^{-1} and Coriolis parameter (f) is 5.8×10^{-5} s^{-1}. L and N stand for a looping, and non-looping track, respectively

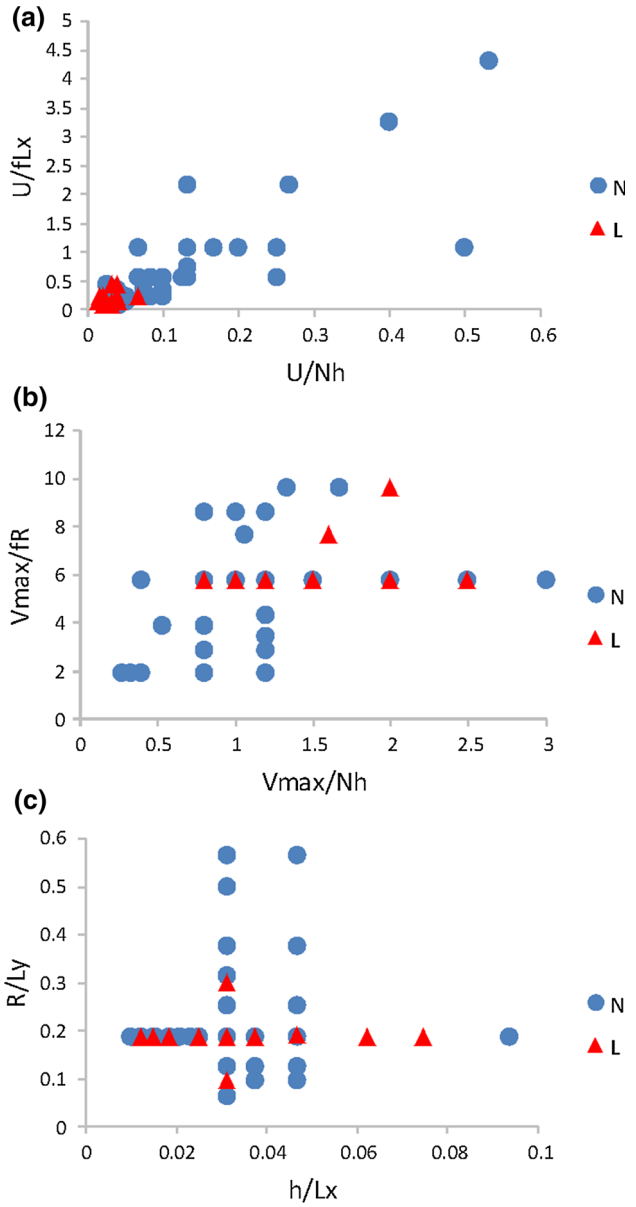

Fig. 1 Looping (*triangles*), and non-looping (*circles*) tracks in the parameter spaces of **a** (U/Nh, U/fL_x), **b** (V_{max}/Nh, V_{max}/fR), and **c** (h/L_x, R/L_y)

numerical experiments, are summarized in Table 1. The discussion will be focused on the windward (eastern) side of the mountain.

3 Essential parameters for looping tracks, looping and non-looping regimes, and looping index (LI)

Smaller U requires more output and longer dimensional time in the nondimensional time $Ut/a = 8$ in the numerical study. To accommodate small U and give a big picture in essential parameters of looping tracks, a looping track is defined as follows: a TC approaches the mountain and then makes a complete loop, or moves away from the mountain more than one-half of the track in x-axis, while with its vertical structure maintained, and the zonal scale of the track no less than the meridional scale in the nondimensional time $Ut/a = 8$ (denoted as L in the legend of Fig. 1). For instance, the tracks in the left column and case C10 in Fig. 2 are looping; whereas the others are non-looping. As discussed above, six nondimensional parameters are considered in the numerical experiments in this study: U/Nh, V_{max}/Nh, U/fL_x, V_{max}/fR, R/L_y, and h/L_x. In the numerical experiments, we have extended the ranges of these nondimensional control parameters as large as possible to reveal the necessary conditions to looping tracks. The purpose of this study is not to determine exact looping and non-looping regime boundaries since they are strongly influenced by both physical and numerical factors; instead, the looping regimes are determined to help understand the formation mechanisms for looping tracks.

3.1 Essential parameters associated with looping tracks

Figure 1 reveals the necessary conditions for looping tracks to occur based on a large number of numerical experiments (Table 1), which shows that the necessary conditions for looping tracks to occur are: $U/Nh \leq 0.067$, $0.8 \leq V_{max}/Nh \leq 2.5$, $U/fL_x \leq 0.43$, $V_{max}/fR \geq 5.7$, $0.094 \leq R/L_y \leq 0.3$, and $0.013 \leq h/L_x \leq 0.075$. The physical meaning of requiring relatively smaller U/Nh, R/L_y and a large enough h/L_x is that *looping tracks require strong orographic blocking*. In particular, *looping tracks demands* very small U/Nh, and U/fL_x (Fig. 1a), which correspond to *very small U dimensionally* (Table 1). Also, the

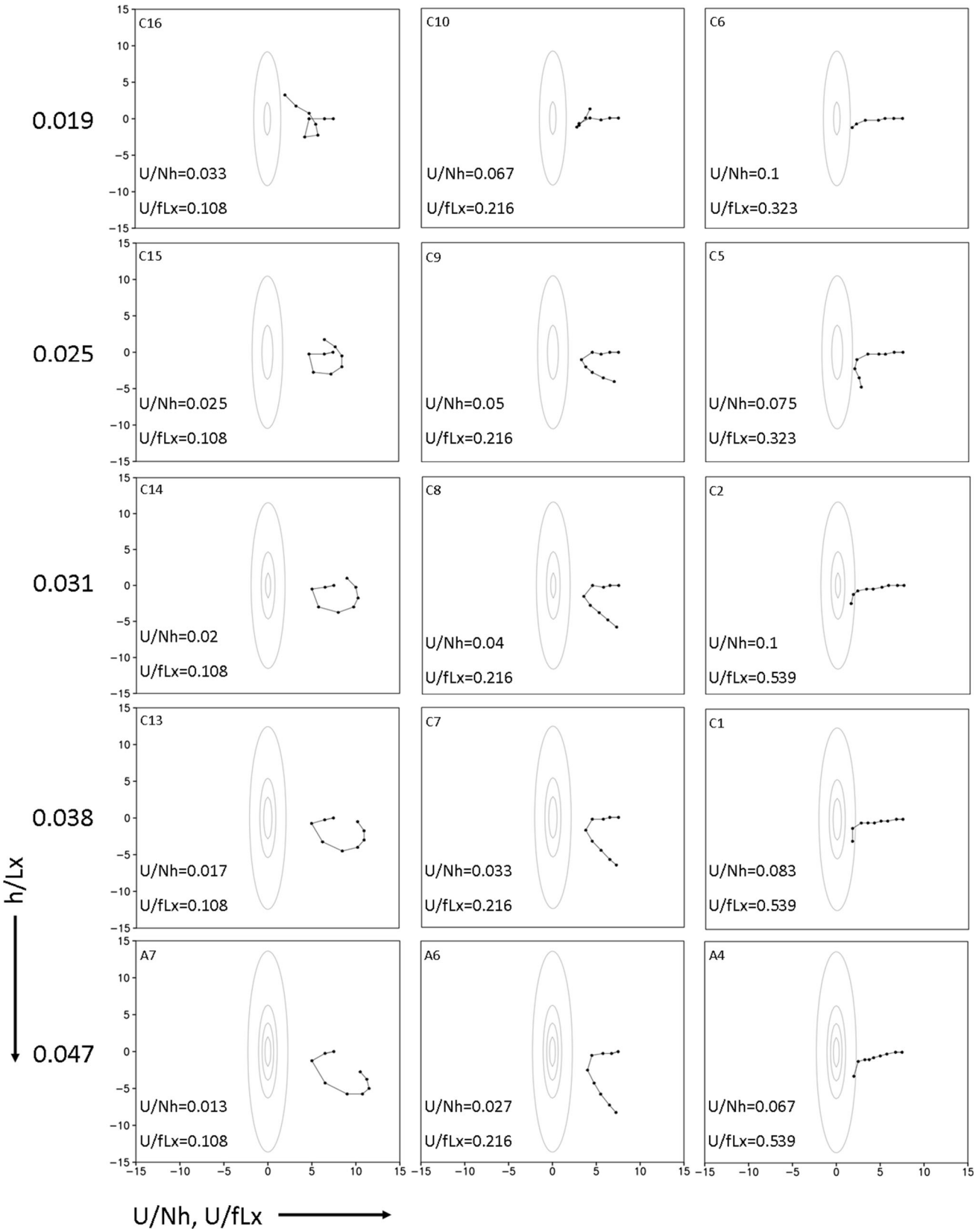
C16
U/Nh=0.033
U/fLx=0.108
C10
U/Nh=0.067
U/fLx=0.216
C6
U/Nh=0.1
U/fLx=0.323
C15
U/Nh=0.025
U/fLx=0.108
C9
U/Nh=0.05
U/fLx=0.216
C5
U/Nh=0.075
U/fLx=0.323
C14
U/Nh=0.02
U/fLx=0.108
C8
U/Nh=0.04
U/fLx=0.216
C2
U/Nh=0.1
U/fLx=0.539
C13
U/Nh=0.017
U/fLx=0.108
C7
U/Nh=0.033
U/fLx=0.216
C1
U/Nh=0.083
U/fLx=0.539
A7
U/Nh=0.013
U/fLx=0.108
A6
U/Nh=0.027
U/fLx=0.216
A4
U/Nh=0.067
U/fLx=0.539
0.019
0.025
0.031
0.038
0.047
h/Lx
U/Nh, U/fLx

◀**Fig. 2** Several cyclone tracks with nondimensional time interval $\Delta Ut/a$ changing with h/L_x, U/Nh, and U/fL_x show two regimes: looping (cases in the *left column* and C10), and non-looping (the other cases). In these numerical experiments, h/L_x increases downward; U/Nh and U/fL_x increases rightward. Both x-axis and y-axis are nondimensionalized by the half-width of the topography in the x-direction (a) hereafter. The cyclone in all cases starts at (7.5, 0). The *oval contours* denote terrain with interval 1000 m

distribution of looping cases shown in Fig. 1b indicates that looping tracks occur under relatively larger V_{max}/fR, moderate V_{max}/Nh, and h/L_x, which reflects the need of large V_{max}. Physically, large V_{max} means that the strong spinning of the typhoon vortex will help prevent the typhoon structure from being destroyed.

Generally speaking, *at a given h/L_x it requires stronger orographic blocking to have a looping track than a non-looping track* (Fig. 2). We studied the cyclone tracks by varying U/Nh and U/fL_x for several h/L_x's. Figure 2 clearly shows that at a fixed V_{max}/Nh, V_{max}/fR, h/L_x, and R/L_y in every row, looping tracks tend to occur and become more pronounced as U/Nh and U/fL_x *decrease*. In other words, looping tracks become more apparent as orographic blocking and Coriolis force increase. When a TC is strongly influenced by orographic blocking, the TC movement is reduced significantly, leading to a weaker Coriolis force. Therefore, the TC movement is driven by subgeostrophic flow. This is consistent with theoretical studies (e.g., reviews in Smith 1979; Lin 2007) and the

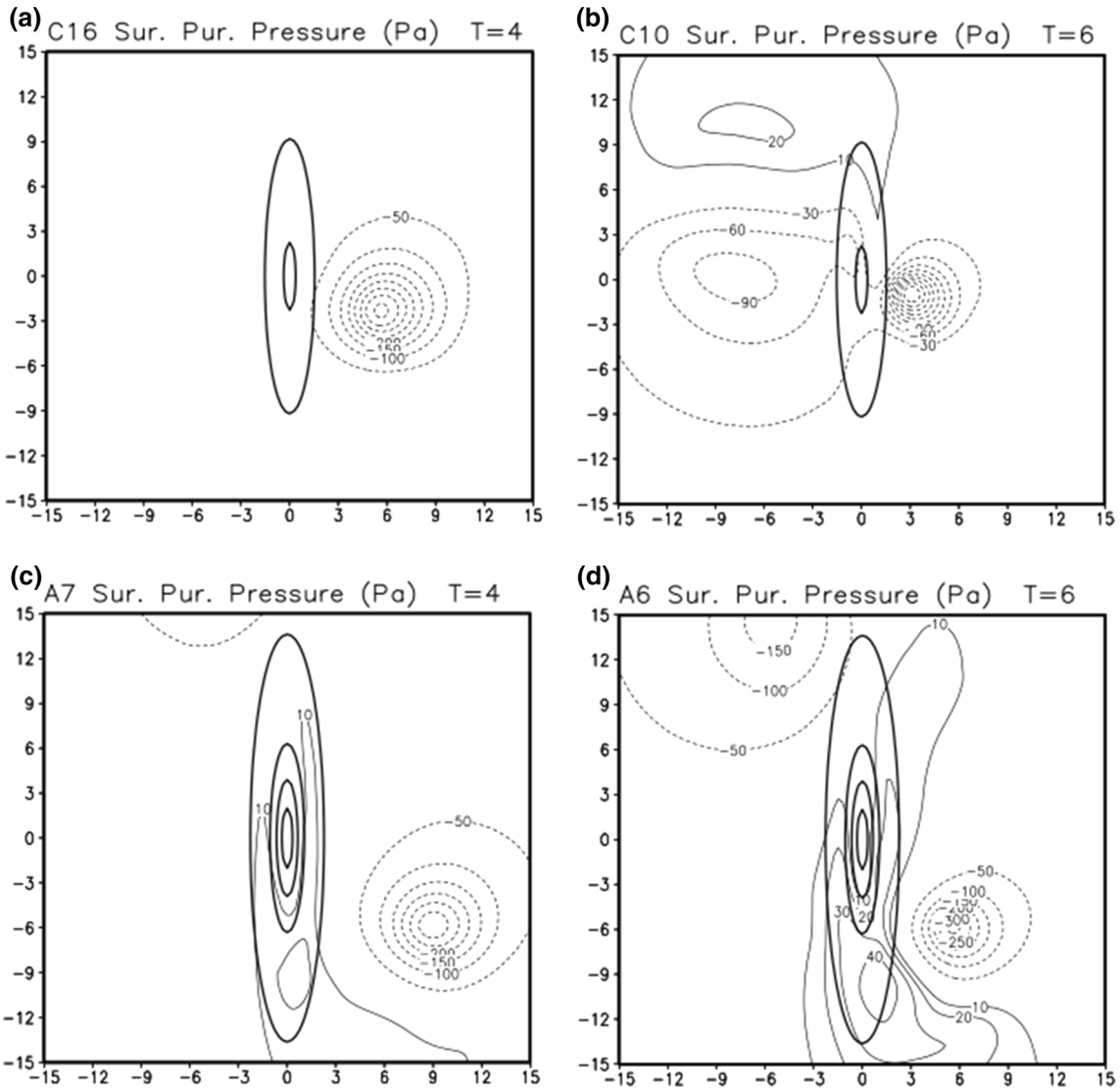

Fig. 3 Surface pressure perturbation of cases **a** C16, **b** C10, **c** A7, and **d** A6. The T in every *panel* denotes the nondimensional time Ut/a. Positive contours are shown as *solid lines*; while negative contours are *dashed lines*. The terrain contour interval is 1000 m

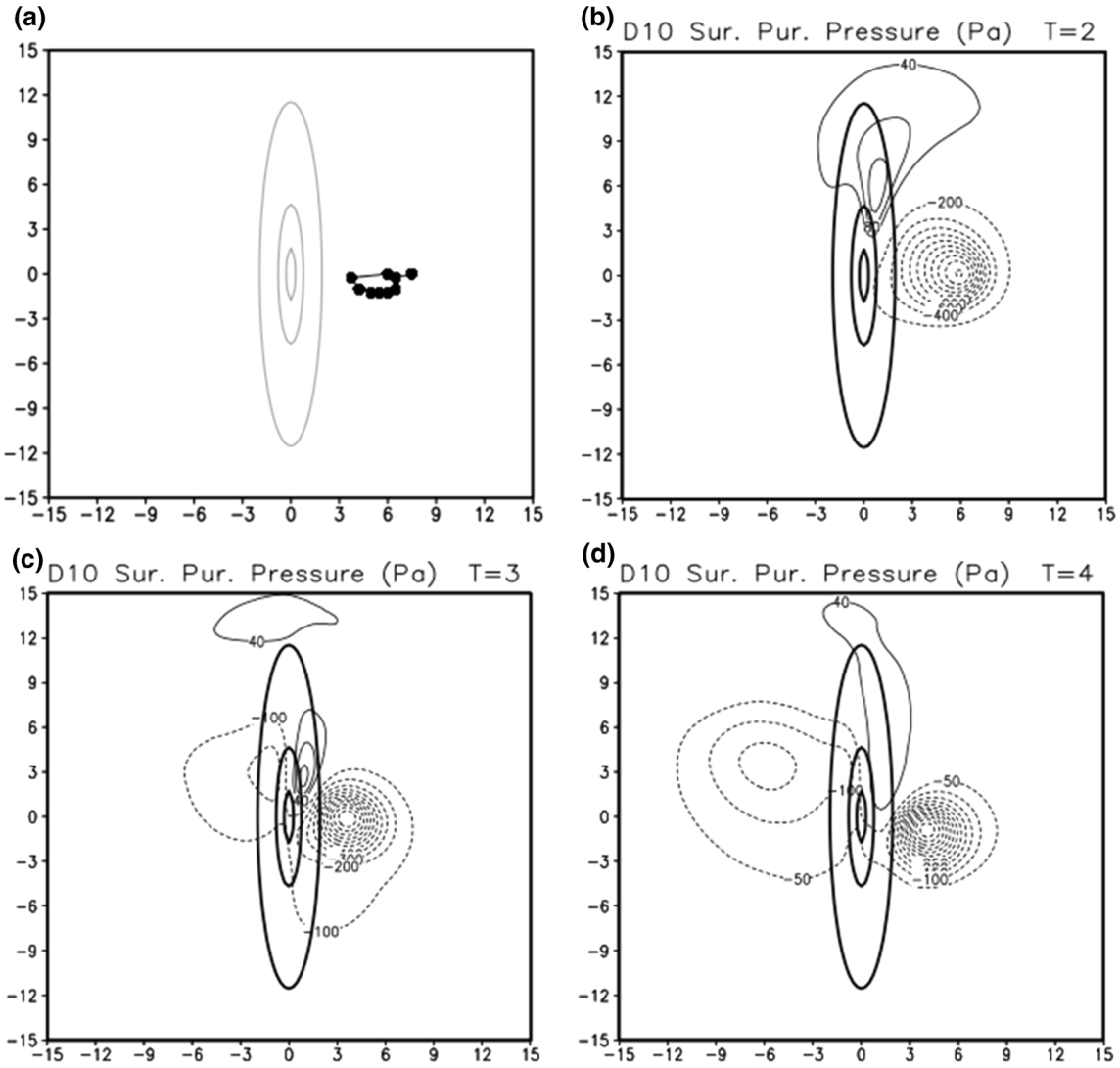

Fig. 4 **a** The cyclone tracks (*black*) and the surface pressure perturbation (Pa) of case D10 at nondimensional time, **b** $Ut/a = 2$, **c** $Ut/a = 3$, and **d** $Ut/a = 4$. Positive contours of surface pressure perturbation at intervals of 40 Pa are shown as *solid lines*; while negative contours are *dashed lines*. The terrain contour interval is 1000 m

observation that TCs slowed down before changing moving directions dramatically.

Furthermore, *moderate steepness* (h/L_x) *favors looping tracks*. In the left and central column cases of Fig. 2, looping tracks are more obvious as h/L_x decreases (dimensional h decreases), and U/Nh and V_{max}/Nh increase when other parameters are the same. There is no looping if a TC approaches a mountain with a very gentle slope (small h/L_x) (e.g., cases C11–C12 vs. C7–10 in Table 1). Also, a TC encountering a mountain with a steep mountain (larger h/L_x) (e.g., cases A7 and A6 in Fig. 2) causes stronger perturbation high pressure existing for a longer time over the northeastern part of mountain, thus the cyclone is pushed farther away from the mountain and stays southward than the cases with smaller value of h/L_x (e.g., cases C16 vs. A7, and C10 vs. A6 in Fig. 3), and then brings on a less obvious looping track than those with a smaller value of h/L_x (e.g., cases C16 vs. A7, and C10 vs. A6 in Fig. 2). Therefore, moderate steepness (h/L_x) favors looping tracks. This is consistent with the looping pattern of V_{max}/Nh in that the conditions with very large or very small value of V_{max}/Nh or h/L_x cannot have a looping track (Fig. 1b, c).

A strong vortex (*large* V_{max}/Nh) *favors looping tracks, too* (Fig. 1b). Stronger maximum tangential velocity (e.g., 50 m s^{-1} in D10 vs. 30 m s^{-1} in C8) leads to weakening of the cyclone dramatically (from 200 to 50 Pa in Fig. 4b–d vs. 100 Pa in Fig. 5a–c), which in turn causes greatly weakening orographic blocking (Fig. 4d) although at first the perturbation high pressure is much stronger (Fig. 4b) than in case C8 (Fig. 5a–d). Thus, the track of case D10

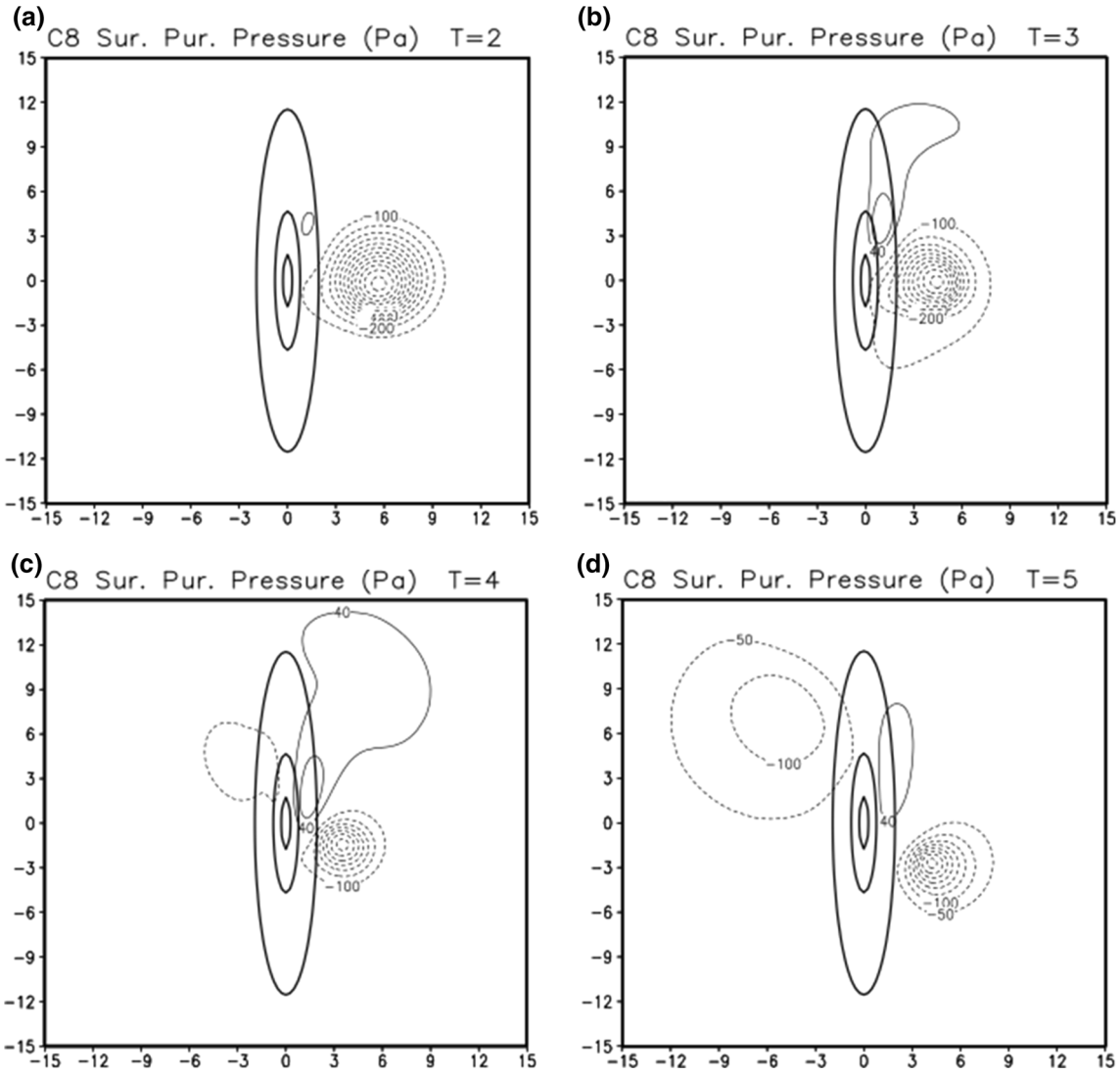

Fig. 5 The surface pressure perturbation of case C8 at the nondimensional time **a** $Ut/a = 2$, **b** $Ut/a = 3$, **c** $Ut/a = 4$, and **d** $Ut/a = 5$ from the GFDM. Positive pressure perturbation is contoured every 40 Pa (*solid*) while negative pressure perturbation is with varying contour intervals (*dashed*). The terrain contour interval is 1000 m

(Fig. 4a) is looping in a different way from case C8 (as in Fig. 2), although these two cases share the same basic flow speed ($U = 1$ m s^{-1}). Due to the impacts of steep steepness (h/L_x), cases D8 and D9 with strong maximum tangential velocity do not have a clear looping track as case D10 (Table 1). However, the influence of large maximum tangential velocity in cases D8–D10 on looping tracks are prominent especially compared with small maximum tangential velocity in cases D5–D7 (not shown). Note the importance of strong vortex requires a condition that orographic blocking is strong enough to keep the TC from passing over the mountain (e.g., $V_{max}/Nh = 3$ in Fig. 2b and cases B5 C4, C12, C18, C20 in Table 1).

Briefly speaking, small basic flow, moderate steepness, and large maximum tangential velocity are three critical parameters for generating a looping track and share the same dynamical process as the blocking exerted by the perturbation high pressure to the east of the mountain.

3.2 The comparison between looping, and non-looping regimes

In the previous subsection, we found small U/Nh and U/fL_x are two most essential necessary criteria for looping tracks among the six non-dimensional parameters (Fig. 1). Physically, small U/Nh indicates the importance of strong orographic blocking; while small U/fL_x shows that looping is greatly affected by the Coriolis force. The combination of strong orographic blocking and the Coriolis force is closely associated with a looping track. Based on the orographic blocking and force balances, a conceptual model for looping tracks is as follows: (1) weak

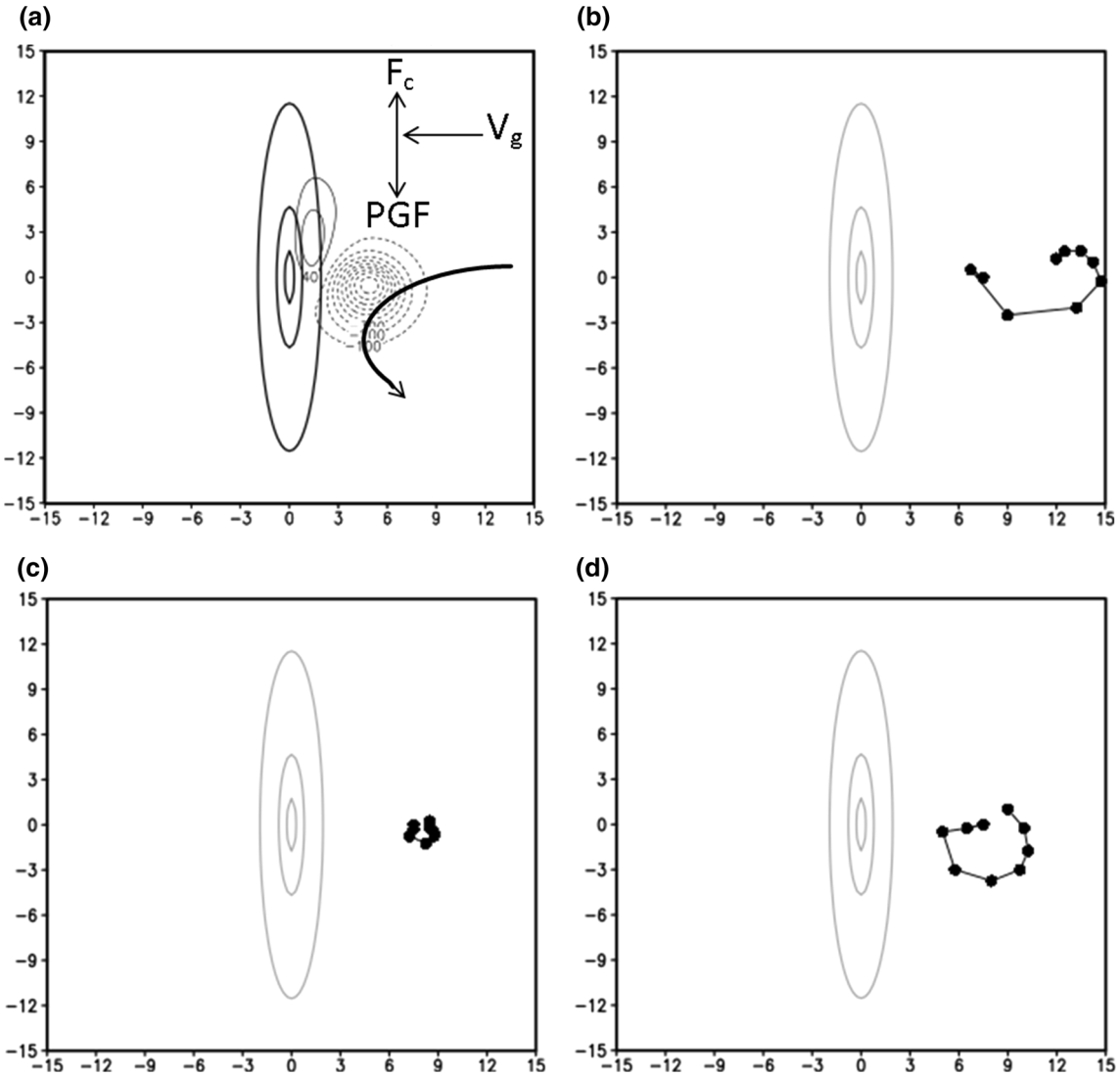

Fig. 6 **a** Conceptual model illustrating the effects of excessive pressure gradient force (PGF) over the Coriolis force as a tropical cyclone (TC) passes over a mesoscale mountain. The *solid* and *dash lines* denote positive and negative pressure perturbation, respectively, of case C14 at nondimensional time $Ut/a = 2$ as an example. The incoming flow (V_g) is in geostrophic balance. The curve denotes the TC track. The TC is steered to loop by the excessive PGF over the Coriolis force. The roughly estimated tracks at nondimensional time interval $\Delta Ut/a$ driven by **b** PGF, and **c** both PGF and the Coriolis force within the radius of 170 km justify the conceptual model. **d** The cyclone track of case C14 from nondimensional time $Ut/a = 0$ to $Ut/a = 8$. The terrain contour interval is 1000 m

orographic blocking. When orographic blocking is weak, advection dominates and the cyclone simply passes over the mountain with insignificant deflection. The cyclone track belongs to the non-looping regime. (2) Moderate orographic blocking. When both orographic blocking and advection are moderate (e.g., $0.1 \geq U/Nh \geq 0.067$, $0.539 \geq U/fL_x \geq 0.323$ in cases A4, C1, C2, C5, and C6 in Fig. 2), the cyclone deflects southward along the mountain. The cyclone track belongs to the non-looping regime. (3) Strong orographic blocking. When orographic blocking is important (e.g., $U/Nh \leq 0.067$, $0.216 \geq U/fL_x \geq 0.108$ in cases A7, C13–C16, and C10 in Fig. 2), originally the cyclone movement is in geostrophic balance but become subgeostrophic due to strong orographic blocking. The zonal displacement reduces as the TC moves closer to the mountain. That the excessive pressure gradient force outweighs the reduced the Coriolis force produces a cyclonic looping track (Fig. 6a). A roughly estimated track at nondimensional time interval $\Delta Ut/a$ driven by net pressure gradient force or the net Coriolis force within the radius of 170 km justify the conceptual model (Fig. 6b–d). Therefore, the strong orographic blocking and subgeostrophic flow result in a looping track (e.g., cases A7, C13–C16 in Fig. 2). The cyclone track belongs to the looping regime.

Figures 7 and 8 illustrate the differences in pressure field between looping and non-looping regimes. Given

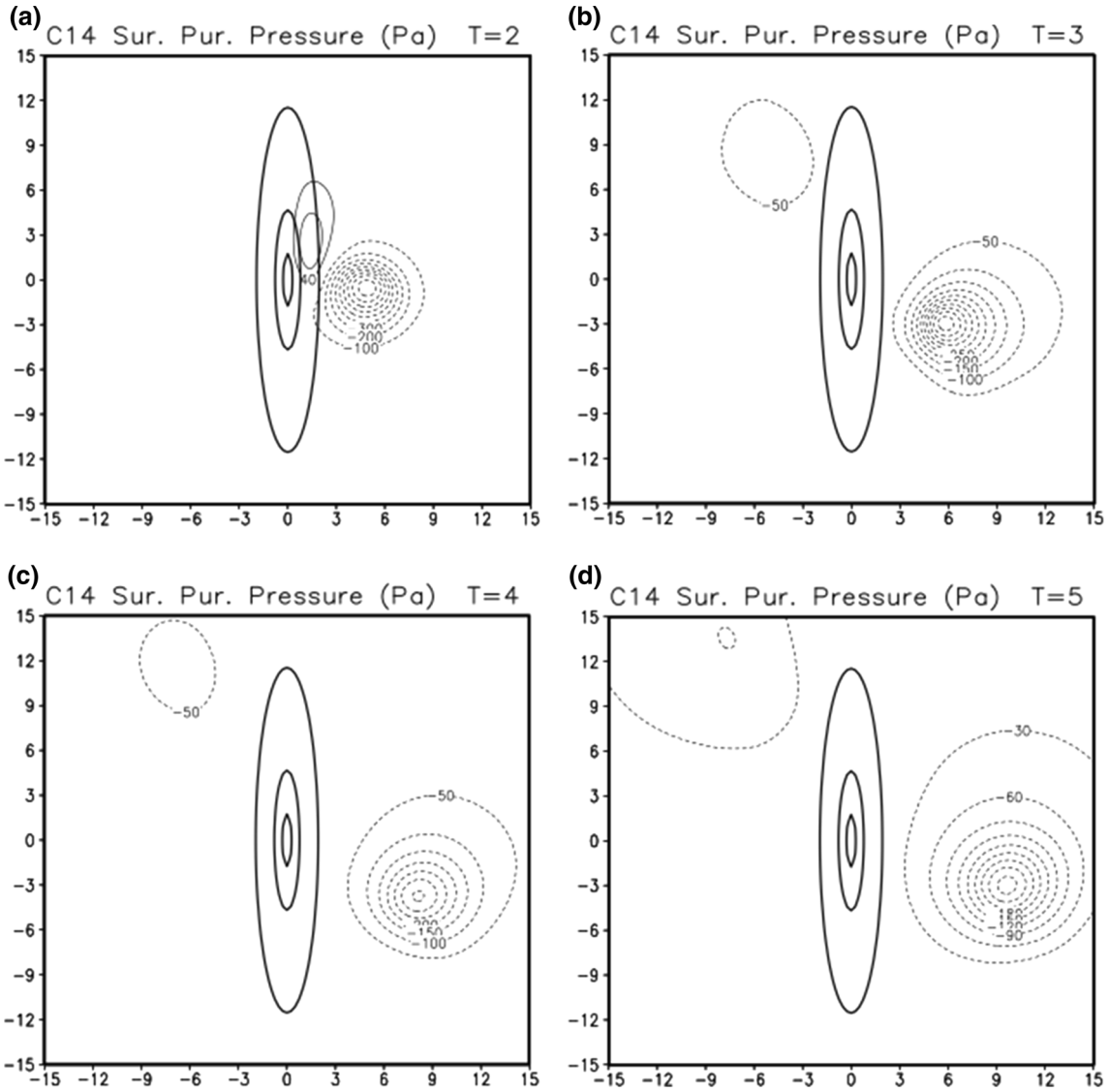

Fig. 7 As in Fig. 5, but for case C14

smaller U/Nh (=0.02), U/fL_x (=0.108), and h/L_x (=0.0313) with larger V_{max}/Nh (=1.2) (e.g., case C14), the advection of cyclone can be ignored, and the orographic blocking is so strong as to slow down and change the direction of the cyclone movement (i.e. the change in track from $Ut/a = 2$ to $Ut/a = 3$ in Fig. 2), and gradually makes a cyclonic looping as a result of strong orographic blocking and the subgeostrophic flow. The perturbation high pressure over the northeastern part of the mountain weakens and then disappears because the cyclone moves away in the looping (Fig. 7). It is very different that given larger U/Nh (=0.067), U/fL_x (=0.539), and h/L_x (=0.0469), together with smaller V_{max}/Nh (=0.8) (e.g., case A4), in which the basic flow is strong leading to stronger inertial force, the inertial force is important. Also, the orographic blocking is strong. Consequently, the cyclone gradually moves slightly southward, and finally weakens. The perturbation high pressure becomes larger and larger in response to the wind field of the long-staying cyclone (Fig. 8).

Figure 9 shows the differences in surface vertical vorticity, wind vectors, and vertical cross sections of perturbation vertical velocity and potential temperature between looping and non-looping regimes. An environmental negative vorticity accompanying the cyclone is originally generated by vorticity shrinking to southeast of the mountain in both looping (C14, Fig. 9a) and non-looping (A4, Fig. 9b) cases stemmed from mass accumulation in lower layers (Fig. 9c, d) due to the orographic blocking and formation of the northerly jet (Fig. 9a, b). Then one child vorticity splits from the negative vorticity and moves along with the cyclone after $Ut/a = 3$ in case C14 (not shown). The northerly jet and negative vorticity around the

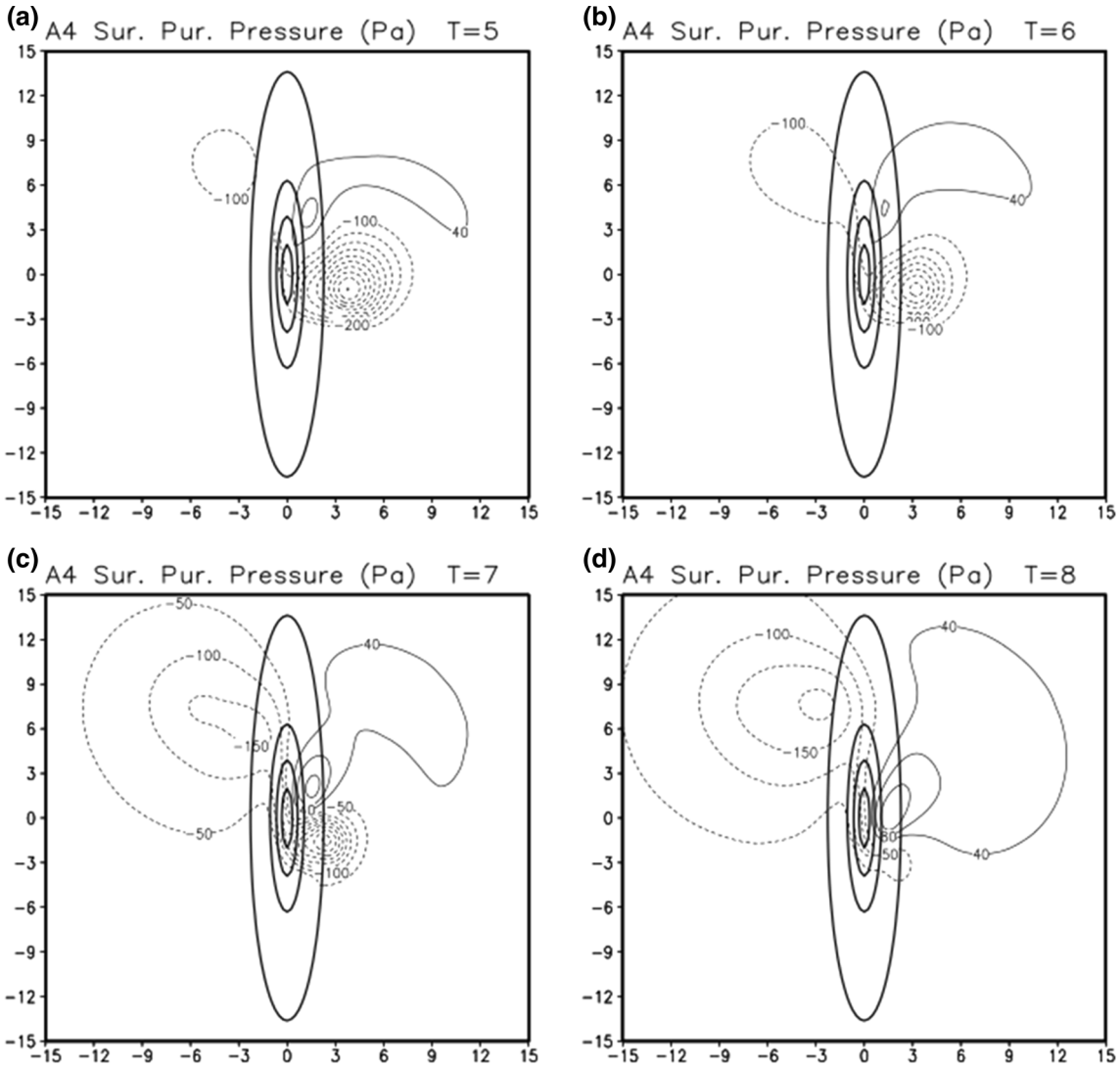

Fig. 8 The surface pressure perturbation of case A4 at the nondimensional time **a** $Ut/a = 5$, **b** $Ut/a = 6$, **c** $Ut/a = 7$, and **d** $Ut/a = 8$. Positive pressure perturbation is contoured every 40 Pa (*solid*) while negative pressure perturbation is with varying contour intervals (*dashed*). The terrain contour interval is 1000 m

southwestern mountain exist in both looping and non-looping cases. In fact, the northerly jet is a common phenomenon as a TC approaches a mesoscale mountain rather than a specialty of looping typhoons (e.g., Jian and Wu 2008; Huang et al. 2011), thus does not serve as a necessary condition or criterion.

3.3 The looping index

As discussed earlier, the occurrence of looping tracks is controlled by the six nondimensional parameters. Can these six nondimensional parameters, U/Nh, V_{max}/Nh, U/fLx, V/fR, h/Lx, and R/Ly, be consolidated into a single control parameter or index for looping tracks? This may be addressed by conducting scatterplot matrix of the looping or non-looping tracks. The procedures of finding out such an index are as follows. First, we conducted scatterplot matrix to find the correlation between these nondimensional parameters. The matrix actually shows that these nondimensional parameters are independent (not shown). Second, we constructed a number of potential looping indices by combining nondimensional parameters according to our numerical experiments, or dimensional variables based on empirical tests. Third, we verified these index candidates by observational data of looping and non-looping typhoons to decide the best one as the looping index.

Based on the necessary conditions of looping tracks as presented in Sect. 3.1, we propose the looping index (LI) as the following

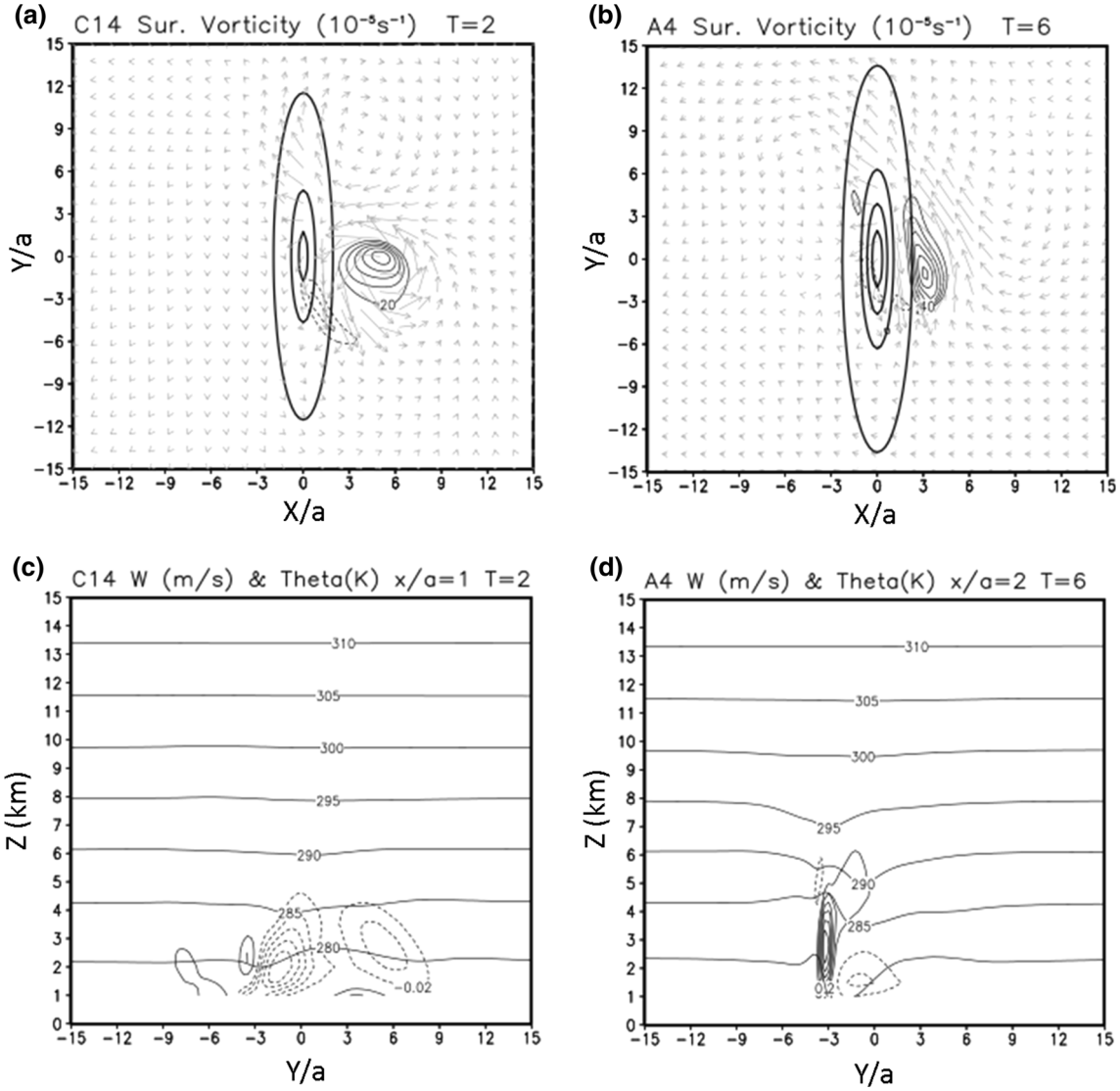

Fig. 9 **a** The surface vertical vorticity and wind vectors, and **c** vertical cross sections of perturbation vertical velocity and potential temperature of case C14 at $x/a = 1$ at the nondimensional time $Ut/a = 2$. **b**, **d** Similar to **a**, **c**, respectively, except for case A4 at $x/a = 2$ at the nondimensional time $Ut/a = 6$. Positive contours are shown as *solid lines* while negative contours are *dashed lines*. The x and y scales are nondimensionalized by a, the mountain half-width in the x-axis. The terrain contour interval is 1000 m

$$\mathrm{LI} = \frac{\frac{U}{Nh}\frac{U}{fL_x}\frac{R}{L_y}}{\frac{V_{\max}}{Nh}\frac{V_{\max}}{fR}\frac{h}{L_x}} = \frac{U^2R^2}{V_{\max}^2 hL_y}. \quad (3)$$

For a TC approaches CMR at an angle θ, the updated meridional half-width in the looping index becomes

$$\widehat{L_y} = L_y \cos(\theta - \pi/6),, \quad (4)$$

where θ is the angle between incident TC and the horizon as measured from the west, and the $\pi/6$ is the approximate orientation of CMR measured from the north. To investigate the importance of these six nondimensional parameters, we calculated the looping index according to Eqs. (3) and (4), for several real typhoon cases. The maximum computed looping index in the looping cases and the minimum estimated looping index in the non-looping cases in the numerous numerical experiments serve as a criterion of looping typhoons and non-looping typhoons, respectively. The typhoon data are obtained from the Digital Typhoon (Kitamoto 2005). The $V_{\max}$ and the radius of $V_{\max}$ were acquired from the Joint Typhoon Warning Center.

Previous studies have shown the looping tracks of Sinlaku (2008) (Fig. 3 in Wu et al. 2013), Krosa (2007), and Haitang (2005) (Fig. 1a in Huang et al. 2011). The looping index, an application of the necessary conditions, is powerful since in general, it is able to successfully differentiate the looping Typhoons Sinlaku (2008), Krosa (2007), and Hitang (2005) (Fig. 10), from the non-looping Typhoons Matmo (2014), Soulik (2013), Nanmadol (2011), and

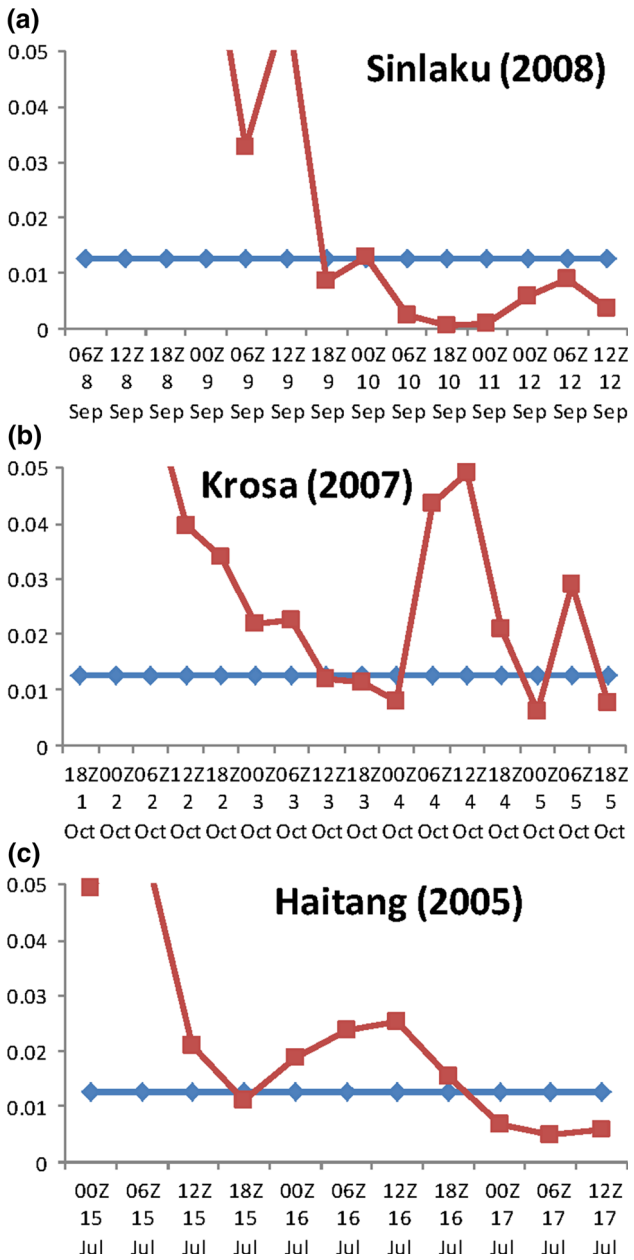

Fig. 10 The calculated looping indexes (*square*) of **a** Typhoon Sinlaku (2008), **b** Typhoon Krosa (2007), and **c** Typhoon Hitang (2005). The maximum computed looping index (0.0125, *diamond*) in the looping cases of the numerous numerical experiments serves as a criterion. The estimated looping indexes from real cyclones below the criterion indicate looping tracks. If the movements of typhoon did not head to CMR at some points, then the looping index was not calculated

Morakot (2009) (Fig. 11) especially when the TC was close to Taiwan. Based on the tests in looping and non-looping cases (Figs. 10, 11), *overall, we may adopt* $LI < 0.0125$ *as the criterion for TC looping track to occur*. Note that the overlapping region between 0.0125 and 0.0047 indicates that our understanding of looping tracks is not quite complete and the construction of the TC LI is not perfect. Therefore, more investigation into the looping track dynamics and better constructions of the looping index are needed.

4 Conclusions and discussion

In this study, we employed the Geophysical Fluid Dynamics Model to conduct idealized numerical experiments to explore the looping track of a westward moving tropical cyclone approaching a mesoscale topography based on a set of nondimensional parameters, U/Nh, V_{max}/Nh, U/fL_x, V_{max}/fR, h/L_x, and R/L_y.

It is found that looping tracks tend to occur under (1) small U/Nh and U/fL_x, (2) moderate h/L_x, and (3) large V_{max}. Physically, the first criterion, i.e. small U/Nh and U/fL_x, corresponds to slow movement (small U), which leads to subgeostrophic flow associated with strong orographic blocking. The cyclonic turning is explained by strong orographic blocking and track deflection associated with the subgeostrophic flow to make a cyclonic turning due to strong orographic blocking, i.e. small U/Nh and R/L_y, along with sufficient large h/L_x. Briefly speaking, the combination of strong orographic blocking and the subgeostrophic flow, in which the excessive pressure gradient force exceeds the reduced Coriolis force, results in a looping track. In addition, looping tracks are more pronounced as h/L_x decreases, U/Nh increases, and V_{max}/Nh increases.

The second criterion, moderate h/L_x, is an interesting finding. Looping tracks require a moderate steep mountain, instead of a very steep mountain, because the TC tends to move southward, instead of making a loop, when it encounters a very steep mountain. The third nondimensional criterion, large V_{max}/Nh, corresponds large maximum tangential wind (V_{max}) associated a strong TC vortex, which helps maintain the vertical alignment of a TC and prevents the TC structure from being destroyed while it approaches the steep mountain. In summary, the essential nondimensional control parameters listed in (1)–(3) correspond to slow movement, moderate steepness, and strong TC vortex.

It is also found that looping tracks are often accompanied by an area of perturbation high pressure located to the northeast of the mountain, which lasts for only a short period. It appears that the perturbation high pressure tends to push the approaching TC away from the mountain. When this excessive pressure gradient force combines with the southward deflection associated with the subgeostrophic flow induced by strong blocking, the TC tends to go southeastward and starts to make a loop. In addition, it is found that the northerly jet and negative vorticity around the southwestern mountain exist in both looping and non-looping cases. Since the northerly jet is a common

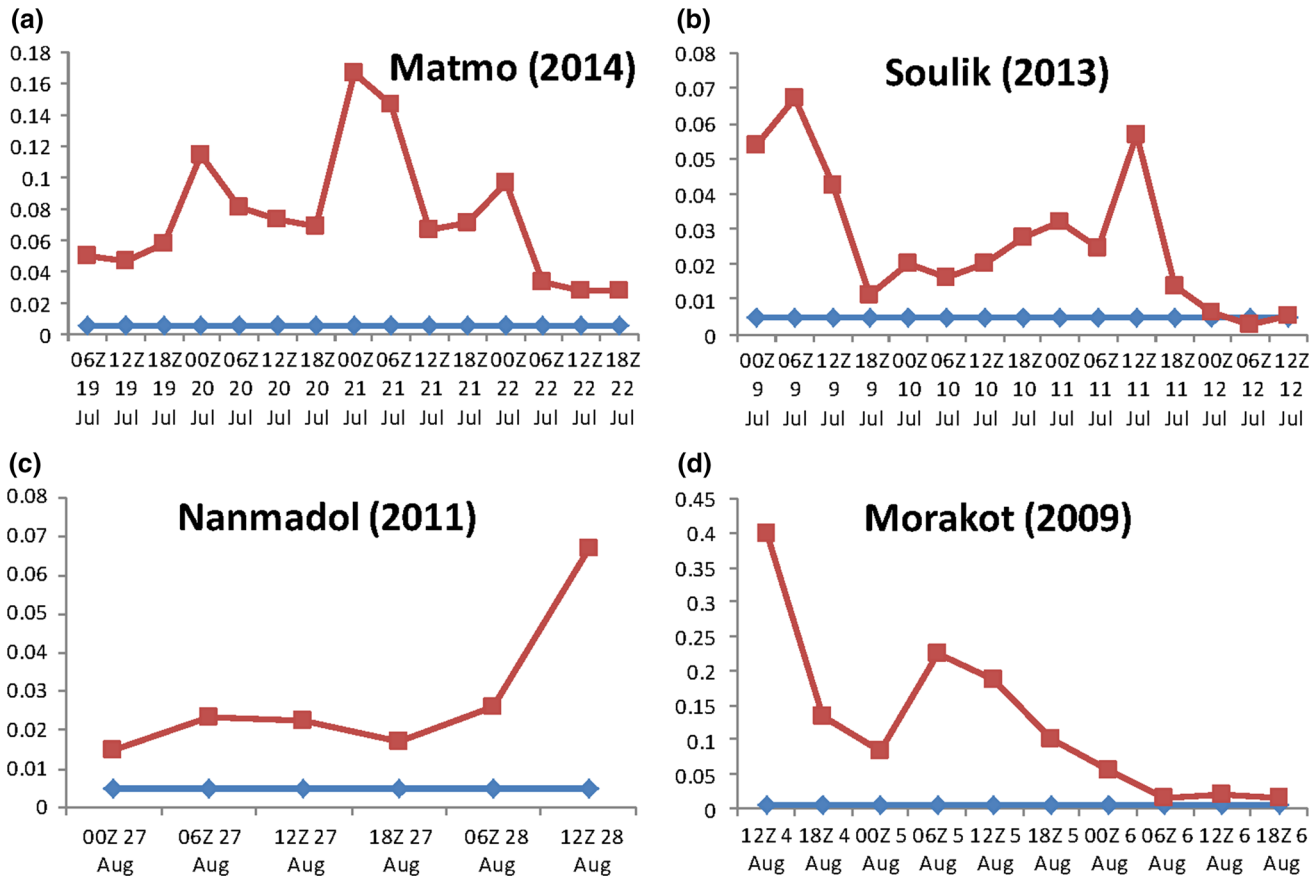

Fig. 11 The calculated looping indexes (*square*) of **a** Typhoon Matmo (2014), **b** Typhoon Soulik (2013), **c** Typhoon Nanmadol (2011), and **d** Typhoon Morakot (2009). The minimum computed looping index (0.0047, *diamond*) in the non-looping cases of the numerous numerical experiments serves as a criterion. The estimated looping indexes from real cyclones above the criterion indicate non-looping tracks. If the movements of typhoon did not head to CMR at some points, then the looping index was not calculated

phenomenon as a TC approaches a mesoscale mountain, it does not serve as a necessary condition or criterion. Based on the above finding, a conceptual model is proposed: (1) weak orographic blocking: the cyclone track belongs to the non-looping regime. (2) Moderate orographic blocking: The cyclone track belongs to the non-looping regime. (3) Strong orographic blocking: The cyclone track belongs to looping regime.

To give a sense of the importance of these six nondimensional parameters, we conducted scatterplot matrix and consolidated the nondimensional control parameters into a TC looping index (LI), $\frac{U^2R^2}{V_{\max}^2 hL_y}$, which was successfully tested by several historical looping and non-looping typhoons approaching Taiwan's CMR from east or southeast. Generally, we may adopt LI < 0.0125 as the criterion for TC looping tracks to occur. Note that even though the proposed looping index is constructed by the six key nondimensional parameters and has been tested by several looping and non-looping typhoon tracks, more testing and improvement are needed.

A complete discussion of the looping track of TCs should further include latent heat, planetary boundary layer processes, sea surface temperature, the variation of Coriolis parameter (i.e., β effect), etc. Nevertheless, the systematic idealized numerical experiments conducted in this study can help understand fundamental dynamics of TC looping tracks and the associated dimensional and nondimensional parameters.

Acknowledgements The authors would like to thank the helpful comments of two anonymous reviewers that led to improvements of the paper. The second author is partially supported by the National Science Foundation Award AGS-1265783.

References

Chang SW-J (1982) The orographic effects induced by an island mountain range on propagating tropical cyclones. Mon Weather Rev 110:1255–1270

Clark TL (1977) A small scale dynamic model using a terrain-following coordinate transformation. J Comput Phys 24:186–215

Gal-Chen T, Sommerville RCJ (1975) On the use of a coordinate transformation for the solution of the Navier–Stokes equations. J Comput Phys 17:209–228

Huang Y-H, Wu C-C, Wang Y (2011) The influence of island topography on typhoon track deflection. Mon Weather Rev 139:1708–1727

Jian G-J, Wu C-C (2008) A numerical study of the track deflection of Supertyphoon Haitang (2005) prior to its landfall in Taiwan. Mon Weather Rev 136:598–615

Kitamoto A (2005) Digital Typhoon: near real-time aggregation, recombination and delivery of typhoon-related information. In: Proceedings of the 4th international symposium on digital earth (ISDE), CD-ROM. http://agora.ex.nii.ac.jp/digital-typhoon/index.html.en

Klemp JB, Durran DR (1983) An upper boundary condition permitting internal gravity wave radiation in numerical mesoscale models. Mon Weather Rev 111:430–444

Lin Y-L (2007) Mesoscale dynamics. Cambridge University Press, Cambridge

Lin Y-L, Han J, Hamilton DW, Huang C-Y (1999) Orographic influence on a drifting cyclone. J Atmos Sci 56:534–562

Lin Y-L, Chen S-Y, Hill CM, Huang C-Y (2005) Control parameters for the influence of a mesoscale mountain range on cyclone track continuity and deflections. J Atmos Sci 62:1849–1866

Lin Y-L, Chen S-H, Liu L (2016) Orographic influence on basic flow and cyclone circulation and their Impacts on track deflection of an idealized tropical cyclone. J Atmos Sci 73:3951–3974

Shapiro R (1970) Smoothing, filtering, and boundary effects. Rev Geophys Space Phys 8:359–387

Smith RB (1979) The influence of mountains on the atmosphere, Advances in Geophysics, vol 21. Academic Press, New York, pp 87–230

Wu C-C, Chen S-G, Lin S-C, Yen T-H, Chen T-C (2013) Uncertainty and predictability of tropical cyclone rainfall based on ensemble simulations of Typhoon Sinlaku (2008). Mon Weather Rev 141:3517–3538

Yang C-C, Wu C-C, Chou K-H, Lee C-Y (2008a) Binary interaction between Typhoons Fengshen (2002) and Fungwong (2002) based on the potential vorticity diagnosis. Mon Weather Rev 136:4593–4611

Yang M-J, Zhang D-L, Huang H-L (2008b) A modeling study of Typhoon Nari (2001) at landfall. Part I: topographic effects. J Atmos Sci 65:3095–3115

Yeh T-C, Hsiao L-F, Chen D-S, Huang K-N (2012) A study on terrain-induced tropical cyclone looping in East Taiwan: case study of Typhoon Haitang in 2005. Nat Hazards 63:1497–1514

Yu H, Huang W, Duan YH, Chan JCL, Chen PY, Yu RL (2007) A simulation study on pre-landfall erratic track of typhoon Haitang (2005). Meteorol Atmos Phys 97:189–206

Zhang D-L, Tian L, Yang M-J (2011) Genesis of Typhoon Nari (2001) from a mesoscale convective system. J Geophys Res 116:D23104